Reduction of metal streak artifacts in x-ray computed tomography using a transmission maximum a posteriori algorithm

B. De Man[1], *Student Member, IEEE* , J. Nuyts[2], *Member, IEEE*, P. Dupont[2], G. Marchal[3], and P. Suetens[1], *Member, IEEE*

[1]Medical Image Computing, Radiology-ESAT/PSI, UZ-GHB, K.U.Leuven, B-3000 Leuven, Belgium
[2]Department of Nuclear Medicine, UZ-GHB, K.U.Leuven, B-3000 Leuven, Belgium
[3]Department of Radiology, UZ-GHB, K.U.Leuven, B-3000 Leuven, Belgium

Abstract

A maximum a posteriori algorithm for reduction of metal streak artifacts in x-ray computed tomography is presented. The algorithm uses a Markov random field smoothness prior and applies increased sampling in the reconstructed image. Good results are obtained for simulations and phantom measurements: streak artifacts are reduced while small, line-shaped details are preserved.

I. INTRODUCTION

Metal artifacts are a major problem in computed tomography (CT). They are caused by the presence of strongly attenuating objects such as dental fillings (figure 1), prosthetic devices, surgical clips, ...

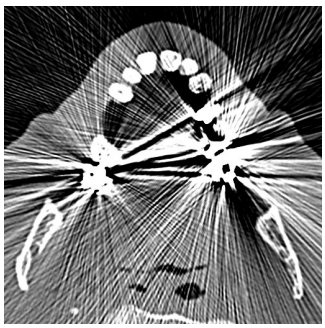

Figure 1: Metal streak artifacts due to the presence of amalgam dental fillings.

Many different approaches for metal artifact reduction (MAR) are found in literature. The most obvious solution is to prevent metal artifacts by using less-attenuating materials (e.g. titanium) or devices with smaller cross-section [1–3]. Haramati [3] showed that using higher energy x-ray beams gives no substantial artifact reduction. Robertson [2, 4] showed that multi-planar reformation allows a better visualization of bone in the presence of metallic orthopedic implants. Henrich [5] applied a post-reconstruction image processing algorithm for removing metal streak artifacts. The majority of MAR-methods consist of a modified reconstruction algorithm, in which metal objects are usually considered opaque and data corresponding to rays through the metal objects are defined as *missing data*. These methods can be divided into two groups:

- Projection completion methods: missing data are replaced by synthetic data, obtained by polynomial or linear interpolation [6–14], pattern recognition [15] or linear prediction methods [16]. Many of these methods apply beam hardening correction as a pre-processing step.
- Iterative methods: existing iterative methods, such as the maximum likelihood expectation maximization (ML-EM) algorithm and the algebraic reconstruction technique (ART), are modified in order to ignore missing data [17–19].

In [20], we have determined the most important sources of metal streak artifacts: noise, non-linear partial volume effect, beam hardening and scatter. Many other sources of artifacts exist (e.g. aliasing, motion, range exceeding) but these appear to be of minor importance under the usual working circumstances.

Our hypothesis is that streak artifacts result from deviations between the true acquisition process and the mathematical model assumed by the reconstruction algorithm. Hence, improving the accuracy of the model should reduce or eliminate the artifacts. If along some projection lines all (or nearly all) photons are attenuated, the projections are incomplete. We hypothesize that the inclusion of some prior knowledge may compensate for this missing information.

This article presents a new algorithm for metal artifact reduction. Further, we show the results of applying this algorithm to simulations and phantom measurements. Finally, we also compare the results of our approach to those obtained by a projection completion method, and to an iterative method that ignores projections through metal inserts.

II. METHODS

A. Algorithm

The algorithm is based on the transmission maximum-likelihood algorithm (ML-TR) published in [21, 22]. ML-TR reconstructs an attenuation image by optimizing the likelihood, assuming that the measured detector read-outs have a Poisson distribution. As a result, ML-TR attributes less weight to low-count detector read-outs, making the algorithm inherently robust against other sources of artifacts that are most prominent in directions of low counts, such as beam hardening, scatter, partial volume effect.

Two extensions are introduced:

1. A Markov random field smoothness prior is used with a Huber potential function [23, 24], given by:

$$\phi(\mu) = \begin{cases} \frac{\mu^2}{2\delta^2} & \text{for } |\mu| \leqslant \delta \\ \frac{|\mu| - \delta/2}{\delta} & \text{for } |\mu| \geqslant \delta, \end{cases} \tag{1}$$

where δ is a positive constant. The Huber function has the advantage of being convex and more or less edge-preserving. The reconstruction in parts of the image for which many high-count measurements are available, is mainly steered by the measured data, while the prior dominates in under-determined parts of the image.

2. Iterations are performed using a reconstruction image at double resolution. After the last iteration, the image is re-sampled to normal resolution. This higher resolution provides a better model for sharp transitions in the image. The increased number of degrees of freedom allows a better handling of other sources of artifacts, such as partial volume effect and beam hardening, and it makes the algorithm more robust.

The logarithm of the posterior probability is given by

$$P = \sum_i \left[y_i \ln B_i - B_i \right] + \sum_j \left[- \sum_{k>j} \left(w_{jk} \phi(\mu_k - \mu_j) \right) \right] , \tag{2}$$

where y_i and B_i represent the measured and calculated counts in detector read-out i, μ_j is the linear attenuation coefficient in pixel j, $w_{jk} = 1$ for adjacent pixels j and k, $w_{jk} = 0$ elsewhere and $\phi(\mu)$ is the potential function.

Using the same gradient algorithm as in [21, 22, 24], namely

$$\mu_j^{n+1} = \mu_j^n - \frac{\frac{\partial P}{\partial \mu_j}}{\sum_\varphi \frac{\partial^2 P}{\partial \mu_j \partial \mu_\varphi}} , \tag{3}$$

where n is the iteration number, the following update formula is obtained:

$$\mu_j^{n+1} = \mu_j^n + \frac{\sum_i \left[c_{ij} (B_i - y_i) \right] + \sum_{k \neq j} \left[w_{kj} \cdot \frac{\partial \phi}{\partial \mu} \Big|_{\mu_k - \mu_j} \right]}{\sum_i \left[c_{ij} (\sum_\varphi c_{i\varphi}) B_i \right]} . \tag{4}$$

We used a projector that interpolates in the image and a back-projector that interpolates in the sinogram.

B. Simulations

Our CT simulator is described and validated in [20]. For the scope of this article, parameters were adjusted to the Siemens Somatom Plus 4 scanner as truthfully as possible. A software phantom is defined as the superposition of a number of objects, each with its own composition, size, position and resolution. We defined a circular Plexiglas phantom (shown in figure 2a), with a diameter of 9.5cm and containing 3 amalgam inserts (ø = 1mm, 2mm and 3mm) and

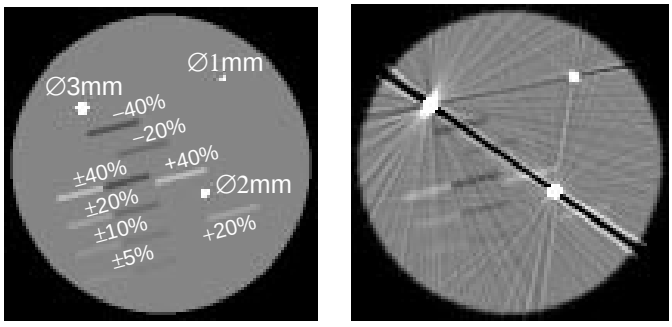

(a) (b)

Figure 2: Simulation: (a) reference image and (b) uncorrected FBP.

12 line-shaped objects (length = 8mm, width = 1 or 2mm, μ=$\pm 40\%, \pm 20\%, \pm 10\%$ or $\pm 5\%$ compared to the attenuation of Plexiglas ; the effective linear attenuation coefficient of Plexiglas is about 0.2cm^{-1}). Simulation was performed at increased sampling, taking into account the continuous rotation of the tube-detector unit and taking into account the finite width of focal spot and detector elements, in order to include the partial volume effect. A poly-chromatic x-ray source was used (by summing 5 discrete energy levels) to include beam hardening. Scatter was simulated by adding a small constant to the simulated intensities. Finally, Poisson noise was included. Figure 2b shows an uncorrected filtered back-projection (FBP) reconstruction of the simulation. All images are 10cm × 10cm, 102 × 102 pixels and are windowed in the interval $\mu = [0.0; 0.4]\ cm^{-1}$.

C. Measurements

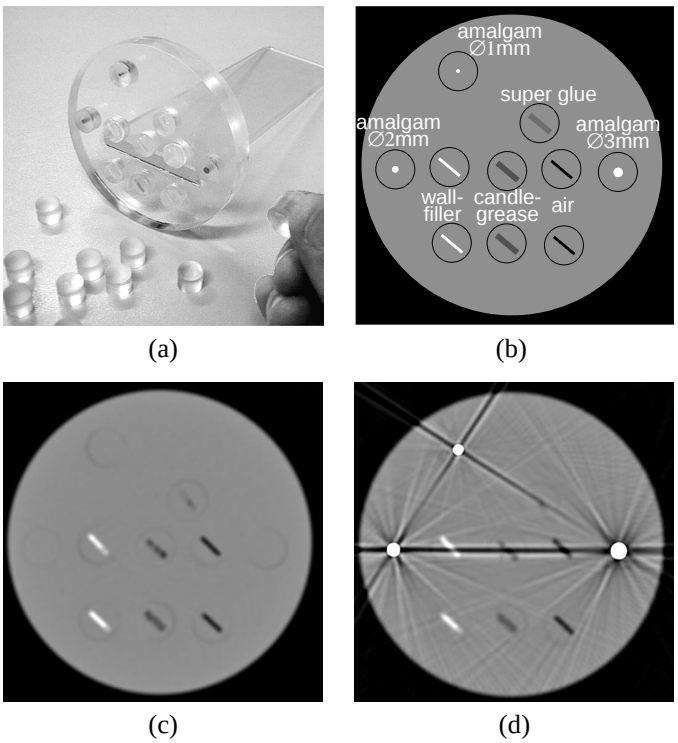

(a) (b)

(c) (d)

Figure 3: Phantom: (a) picture, (b) schematic, (c) FBP without metal, (d) FBP with metal.

We designed a circular Plexiglas phantom (figure 3a),

with thickness 1cm and with a diameter of 9.5cm, similar to the software phantom from the previous paragraph. A number of small Plexiglas cylinders, some of which contain either amalgam fillings or line-shaped objects (candle-grease, air, super glue and wall-filler), can be positioned in holes in the phantom. Figure 3b shows the setup with amalgam fillings. Alternatively, the cylinders with amalgam fillings were replaced by plain Plexiglas cylinders, yielding a setup without metal objects (not shown). The two setups were scanned with a Siemens Somatom Plus4 CT-scanner in sequential scan mode with fixed focal spot, using a nominal tube voltage of 120kV, a tube current of 130mA, a slice thickness of 1.0mm and a 0.75s rotation. All measurements include standard first order beam hardening correction by the scanner. Figure 3 shows the uncorrected FBP reconstructions of the measurements of the setup without (c) and with (d) amalgam fillings.

D. Other algorithms

For comparison, we also applied the following algorithms to the measurements:

Projection completion method [12, 13] :
The metal objects are segmented from an FBP-reconstruction using a threshold of $\mu = 2\text{cm}^{-1}$. This metal-only image is projected, resulting in a metal-only sinogram. Parts of the original sinogram corresponding to non-zero values in the metal-only sinogram are defined as missing data. These missing values are replaced by linear interpolation on a view-by-view basis. The resulting synthetic sinogram is reconstructed using FBP. Finally, the previously segmented metal image is added to the reconstruction.

ML-EM ignoring missing data [18] :
Missing data are defined in the same way as in the projection-completion method. In each iteration, the error sinogram is made zero at the positions of missing data. At the end of the iterations, the previously segmented metal image is added to the reconstruction.

ML-TR ignoring missing data :
Same as ML-EM ignoring missing data.

III. Results

A. Simulations

Figure 4 shows ML-TR reconstructions of the simulation computed at normal resolution (top) and at double resolution followed by re-sampling (bottom), without prior (left) and with a Huber prior (right).

B. Measurements

Figures 5 and 6 show ML-TR reconstructions of the measurements with and without metal objects. Figure 7a shows the FBP reconstruction after projection completion using linear interpolation [12, 13]. Figure 7b shows the ML-EM reconstruction ignoring missing data [18]. Figure 7c shows the ML-TR reconstruction ignoring missing data. Figure 7d repeats the reconstruction obtained with ML-TR at double

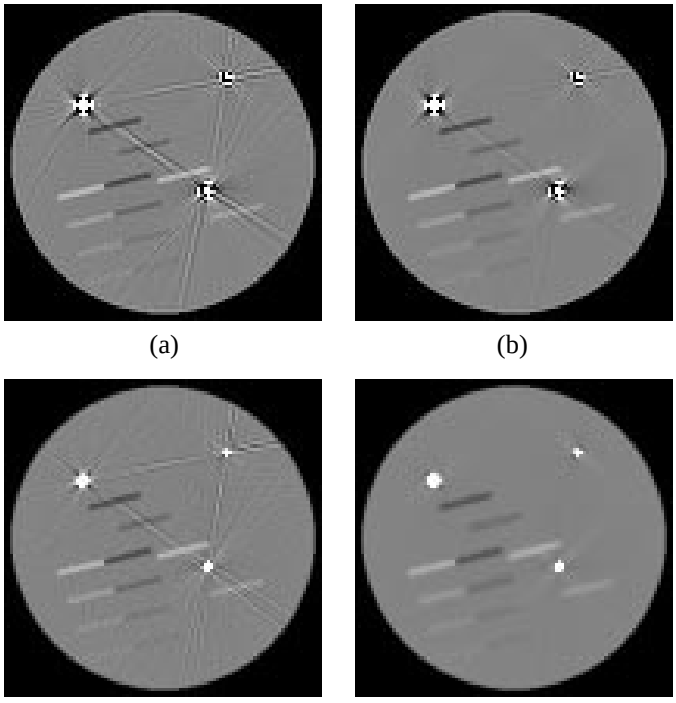

Figure 4: ML-TR reconstructions of the simulation: at single (a, b) and at double (c, d) resolution, without (a, c) and with (b, d) Huber prior.

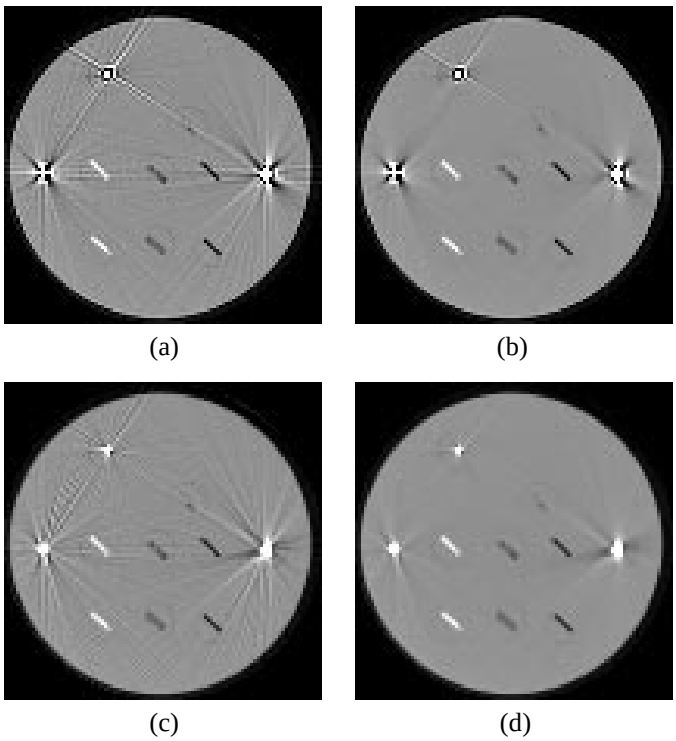

Figure 5: ML-TR reconstructions of the measurement with amalgam fillings: at single (a, b) and at double (c, d) resolution, without (a, c) and with (b, d) Huber prior.

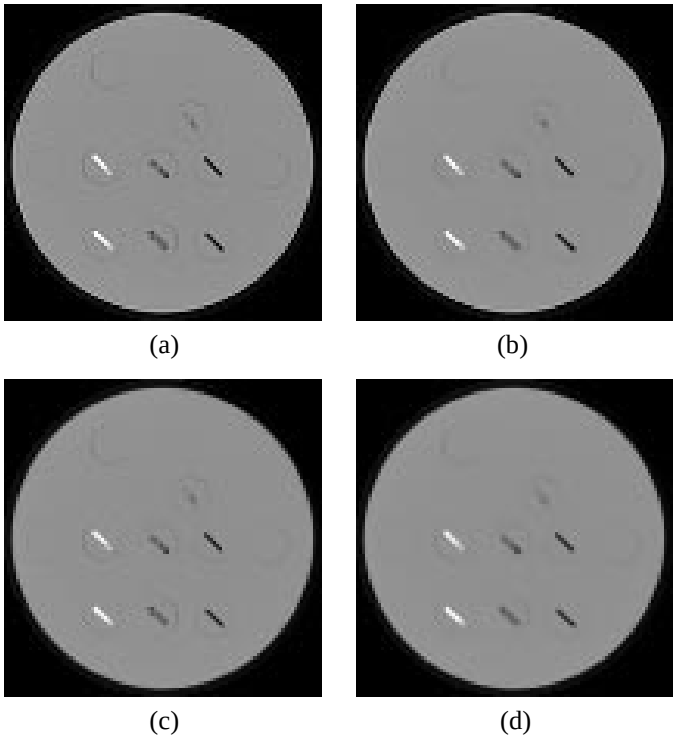

(a) (b)

(c) (d)

Figure 6: ML-TR reconstructions of the measurement without amalgam fillings: at single (a, b) and at double (c, d) resolution, without (a, c) and with (b, d) Huber prior.

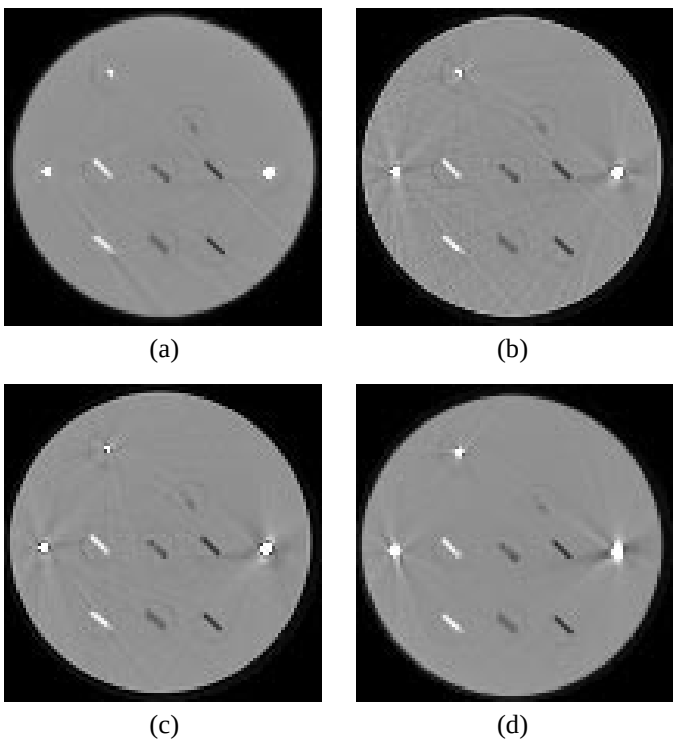

(a) (b)

(c) (d)

Figure 7: (a) FBP after projection completion. (b) ML-EM ignoring missing data. (c) ML-TR ignoring missing data. (d) ML-TR at double resolution with Huber prior.

resolution with Huber prior.

IV. Discussion

A. Simulations

The circular phantom allows the exclusion of most non-metal-artifacts and to concentrate on pure metal-artifacts. All ML-TR reconstructions in figure 4 exhibit fewer streaks than the FBP reconstruction in figure 2b. This illustrates the robustness of the ML-TR algorithm and the importance of the correct acquisition model. Comparison of the images at the left to those at the right shows the importance of the prior for a good convergence. Comparison of top and bottom images shows the importance of the double resolution reconstruction. ML-TR *with* prior at *double* resolution (figure 4d) gives the best result: the streaks are removed and the line-shaped objects are conserved. Note however that some smoothing is introduced by applying the prior.

B. Measurements

The results in figure 5 are similar to the simulations. All ML-TR reconstructions exhibit less streaks than the FBP-reconstruction in figure 3d. Comparison of the images at the left to those at the right shows the importance of the prior for a good convergence. Comparison of top and bottom images shows the importance of the double resolution reconstruction. ML-TR *with* prior at *double* resolution (figure 5d) gives the best result: streaks are reduced and the line-shaped objects are conserved. Note again that some smoothing is introduced by applying the prior. Also, there are some remaining streaks in the vicinity of the metal objects. Close investigation has shown that these remaining streaks are due to a slight mismatch between our mathematical model and the real scanner (due to some specific design features). This explains why these streaks are not present in the simulations. Further work is required to refine our model. For the measurements without metal objects (figure 6), the double resolution has no effect, and the prior only introduces some smoothing.

For the other methods (figure 7a–c), the quality of the reconstruction in the vicinity of the metals compares favorably with ML-TR at double resolution with Huber prior. On the other hand new streaks are created at other locations in the image. We cannot conclude that our method gives better results than the other methods. Nevertheless, the results confirm our hypothesis that improving the accuracy of the acquisition model reduces metal streak artifacts. More investigation is required to further improve the model of the scanner geometry and to include explicit models for the partial volume effect, scatter and beam hardening.

V. Conclusion

Our simulations indicate that ML-TR reconstruction using a-priori knowledge and using an increased number of degrees of freedom results in effective artifact reduction. Future work will attempt to improve the model of the scanner geometry, in order to reduce the remaining streaks. Additionally, we intend to study the use of explicit models for beam hardening, partial volume effect and scatter. This will allow to reduce the weight

of the prior, offering equally good artifact reduction with less smoothing. More complex phantoms with larger and more attenuating metal objects and with axial gradients must be studied. For application in clinical routine, a strong reduction of the computational cost of the algorithm is required.

VI. Acknowledgments

This work is supported by the Flemish Fund for Scientific Research (FWO), grant number G.0106.98. P. Dupont is post-doctoral researcher of the FWO. We thank the people from the Dept. of Radiology for their help in the experiments. We also thank Els Tijskens for the production of the Plexiglas phantom. Finally, we thank Stefan Schaller (Siemens) for the information on the Siemens CT-scanners.

VII. References

[1] J.A.Veiga-Pires and M.Kaiser, "Artefacts in CT scanning," *Br J Radiol, vol. 52, 1979, pp. 189-204*

[2] D.D.Robertson, P.J.Weiss et al, "Evaluation of CT Techniques for Reducing Artifacts in the Presence of Metallic Orthopedic Implants," *J Comput Assist Tomogr, vol.12, nr.2, 1988, pp.236-241*

[3] N.Haramati, R.B.Staron et al, "CT scans through metal scanning technique versus hardware composition," *Comput Med Imaging Graph, vol.18, nr.6, 1994, pp.429-434*

[4] D.D.Robertson, D.Magid et al, "Enhanced Computed Tomographic Techniques for the Evaluation of Total Hip Arthroplasty," *J Arthr, vol.4, nr.3, 1989, pp.271-276*

[5] G.Henrich, "A simple computational method for reducing streak artifacts in CT images," *Comp Tomo, vol.4, 1980, pp.67-71*

[6] R.M.Lewitt and R.H.Bates, "Image reconstruction from projections: III: Projection completion methods (theory)," *Optik, vol. 50, 1978, pp. 189-204*

[7] T.Hinderling, P.Rüegsegger et al, "Computed Tomography Reconstruction from Hollow Projections: An Application to In Vivo Evaluation of Artificial Hip Joints," *J Comput Assist Tomogr, vol.3, nr.1, 1979, pp.52-57*

[8] G.H.Glover and N.J.Pelc, "An algorithm for the reduction of metal clip artifacts in CT reconstructions," *Med Phys, vol.8, nr.6, 1981, pp.799-807*

[9] P.Seitz and P.Rüegsegger, "Anchorage of Femoral Implants Visualized by Modified Computed Tomography," *Arch Orthop Trauma Surg, vol.100, 1982, pp.261-266*

[10] B.P.Medoff, W.R.Brody et al, "Iterative convolution backprojection algorithms for image reconstruction from limited data," *J Opt Soc Am, vol.73, nr.11, 1983, pp.1493-1500*

[11] P.Seitz and P.Rüegsegger, "CT bone densitometry of the anchorage of artificial knee joints," *J Comput Assist Tomogr, vol.9, 1985, pp.621-622*

[12] W.A.Kalender, R.Hebel et al, "Reduction of CT Artifacts Caused by Metallic Implants," *Radiology, vol.164, 1987, pp.576-577*

[13] E.Klotz, W.Kalender et al, "Algorithms for reduction of CT artefacts caused by metallic implants," *SPIE, vol.1234 Medical Imaging IV, 1990, pp.642-650*

[14] H.K.Tuy, "A post-processing algorithm to reduce metallic clip artifacts in CT images," *Eur Radiol, vol.3, 1993, pp.129-134*

[15] R.L.Morin and D.E.Raeside, "A Pattern Recognition Method for the Removal of Streaking Artifact in Computed Tomography," *Radiology, vol.141, 1981, pp.229-233*

[16] K.Rajgopal, N.Srinivasa et al, "Image Reconstruction from Incomplete Projection Data: a Linear Prediction Approach," *in Medical Imaging Systems Techniques and Applications Modalities, C.T.Leondes, Gordon and Breach Science Publishers, 1997, pp.281-328*

[17] B.E.Oppenheim, "Reconstruction Tomography from Incomplete Projections," *in Reconstruction Tomography in Diagnostic Radiology and Nuclear Medicine, M.M.Ter-Pogossian et al, Eds.Baltimore, University Park, 1977, pp.155-183*

[18] G.Wang, D.L.Snyder et al, "Iterative Deblurring for CT Metal Artifact Reduction," *IEEE Trans Med Imaging, vol.15, 1996, pp.657-664*

[19] D.D.Robertson, J.Yuan et al, "Total Hip Prosthesis Metal-Artifact Suppression Using Iterative Deblurring Reconstruction," *J Comput Assist Tomogr, vol.21, 1997, pp.293-298*

[20] B.De Man, J.Nuyts et al, "Metal Streak Artifacts in X-ray Computed Tomography: A Simulation Study," *IEEE Trans Nucl Sci, vol.46, nr.3, 1999, pp.691-696*

[21] J.Nuyts, P.Dupont et al, "Iterative reconstruction of transmission sinograms with low signal to noise ratio," *in "2nd IEEE Workshop CMP: can we beat the curse of dimensionality (Prague, Czech Republic, Aug.28-30, 1996)"*, Birkhäuser, 1997, pp.237-248

[22] J.Nuyts, B.De Man et al, "Iterative reconstruction for helical CT: a simulation study," *Phys Med Biol, vol.43, 1998, pp.729-737*

[23] E.U.Mumcuoğlo, R.Leahy et al, "Bayesian reconstruction of PET images: methodology and performance analysis," *Phys Med Biol, vol.41, 1996, pp.1777-1807*

[24] J.Nuyts, P.Dupont et al, "Simultaneous maximum a-posteriori reconstruction of attenuation and activity distributions from emission sinograms," *IEEE Trans Med Imaging, vol.18, nr.5, 1999, pp.393-403*